International Journal of Nanomedicine

Dovepress
open access to scientific and medical research

Open Access Full Text Article

ORIGINAL RESEARCH

A novel dendritic nanocarrier of polyamidoamine-polyethylene glycol-cyclic RGD for "smart" small interfering RNA delivery and in vitro antitumor effects by human ether-à-go-go-related gene silencing in anaplastic thyroid carcinoma cells

This article was published in the following Dove Press journal:
International Journal of Nanomedicine
26 March 2013
Number of times this article has been viewed

Guanhua Li[1,2]
Zuojun Hu[1]
Henghui Yin[1]
Yunjian Zhang[1]
Xueling Huang[1]
Shenming Wang[1]
Wen Li[2]

[1]Department of Vascular and Thyroid Surgery, [2]Key Laboratory of Surgery, The First Affiliated Hospital, Sun Yat-sen University, Guangzhou, People's Republic of China

Abstract: The application of RNA interference techniques is promising in gene therapeutic approaches, especially for cancers. To improve safety and efficiency of small interfering RNA (siRNA) delivery, a triblock dendritic nanocarrier, polyamidoamine-polyethylene glycol-cyclic RGD (PAMAM-PEG-cRGD), was developed and studied as an siRNA vector targeting the human ether-à-go-go-related gene (*hERG*) in human anaplastic thyroid carcinoma cells. Structure characterization, particle size, zeta potential, and gel retardation assay confirmed that complete triblock components were successfully synthesized with effective binding capacity of siRNA in this triblock nanocarrier. Cytotoxicity data indicated that conjugation of PEG significantly alleviated cytotoxicity when compared with unmodified PAMAM. PAMAM-PEG-cRGD exerted potent siRNA cellular internalization in which transfection efficiency measured by flow cytometry was up to 68% when the charge ratio (N/P ratio) was 3.5. Ligand-receptor affinity together with electrostatic interaction should be involved in the nano-siRNA endocytosis mechanism and we then proved that attachment of cRGD enhanced cellular uptake via RGD-integrin recognition. Gene silencing was evaluated by reverse transcription polymerase chain reaction and PAMAM-PEG-cRGD-siRNA complex downregulated the expression of *hERG* to 26.3% of the control value. Furthermore, gene knockdown of *hERG* elicited growth suppression as well as activated apoptosis by means of abolishing vascular endothelial growth factor secretion and triggering caspase-3 cascade in anaplastic thyroid carcinoma cells. Our study demonstrates that this novel triblock polymer, PAMAM-PEG-cRGD, exhibits negligible cytotoxicity, effective transfection, "smart" cancer targeting, and therefore is a promising siRNA nanocarrier.

Keywords: small interfering RNA, dendrimer, gene silencing, human ether-à-go-go-related gene, anaplastic thyroid cancer

Introduction

Small interfering RNA (siRNA) is double-stranded RNA with a sequence of 20–25 base pairs, participating in RNA interference (RNAi), which modulates expressions of targeted genes specifically.[1] The application of RNAi techniques for prospective cancer gene therapy has received enormous research devotions.[2] However, cytotoxic insecurity and ineffective transport of siRNA for mammalian cells are major limitations hindering siRNA therapeutic applications.[3] Recent advances in nonviral vectors such as cationic polymers or dendrimers give us some hope in overcoming some of the obstacles for efficient siRNA delivery.

Correspondence: Shenming Wang
Department of Vascular and Thyroid Surgery, The First Affiliated Hospital of Sun Yat-sen University, 58 Zhongshan 2nd Road, Yuexiu District, Guangzhou 510080, People's Republic of China
Tel +86 20 8775 5766 ext 8212
Fax +86 20 8775 5766 ext 8198
Email shenmingwang@vip.sohu.com

Polyamidoamine (PAMAM) dendrimer and its derivatives are nanometer-sized polymers with cationic surface environments, which enable electrostatic interactions and complexations to nucleic acids, like siRNA.[4] By virtue of its specific spherical architecture PAMAM provides multivalent conjugations to cellular surfaces, leading to stronger permeability and more siRNA cargo. As a versatile nanocarrier, PAMAM evidently shows its superiorities, which have been proved by previous research reports, revealing an effective and powerful delivery system in multiple cell lines.[5–8]

Anaplastic thyroid carcinoma (ATC) is the most aggressive malignancy in thyroid cancers and ATC manifests rapid progression, high invasiveness, and early occurrence of metastasis, resulting in a poor prognosis.[9] For ATC, inaccessibility to early diagnosis, and resistance to radiation and chemotherapy are factors handicapping therapeutic strategies; it is therefore urgent to seek for new and potent therapeutic targets.

Human ether-à-go-go-related gene (*hERG*), a member of the ether-à-go-go (EAG) family, encodes specific K^+ channels.[10] *hERG*-dependent K^+ channels, found in various cancerous tissues such as renal neoplasm,[11] neuroblastoma,[12] leukemic cells,[13] and breast carcinoma,[14] are broadly relevant to cell proliferation, apoptosis, differentiation, invasion, and metastasis.[15]

Integrin, well known for its overexpression in plenty of cancer cells, induces adhesion between cell and extracellular matrix (ECM) by specific recognition of Arg-Gly-Asp sequences in the ECM.[16] Cyclic RGD peptide (cRGD) selectively binds integrin protein and may act as a blocker for the pathogenesis of cancer invasion and angiogenesis.[17,18] Cilengitide, a cRGD targeting integrin, has undergone a Phase III clinical trial by Merck and Co., Inc, Whitehouse Station, NJ, USA.[19–21] Moreover, successful examples have confirmed that bioconjugation of dendrimers and cRGD facilitates cellular uptake of therapeutic agents or nanoparticles in cancer cells.[22–24]

Based on this background, in the present study we aimed to design and synthesize a multivalent nanocarrier, PAMAM-polyethylene glycol-cRGD (PAMAM-PEG-cRGD), with three independent blocks, in which PAMAM offered a cationic environment for siRNA binding, PEG improved biocompatibility, and cRGD enhanced endocytosis in tumor cells. The antitumor effects of *hERG* silencing in ATC were also investigated.

Material and methods

Materials

PAMAM generation 4.0 dendrimer (molecular weight [MW] 14,214 Da, 64 amide end groups), 3-(4,5-dimethylthiazol-2-yl)-2,5-diphenyltetrazolium bromide (MTT), L-glutamine, penicillin, streptomycin, ethidium bromide, 4,6-diamidino-2-phenylindole (DAPI), and poly(L-lysine) (PLL) were purchased from Sigma-Aldrich (St Louis, MO, USA). cRGD (MW = 595 Da) was synthesized from GL Biochem Company (Shanghai, People's Republic of China). N-hydroxysulfosuccinimide-PEG-maleimide (NHS-PEG-MAL, MW = 5000 Da) was designed by Nanocs Inc (Boston, MA, USA). β-mercaptoethanol (MW = 78.1 Da), goat anti-*hERG* polyclonal antibody, goat anti-vascular endothelial growth factor (VEGF) polyclonal antibody, and anti-goat second antibody were purchased from Santa Cruz Biotechnology Inc (Santa Cruz, CA, USA). Rabbit anti-cleaved caspase-3 polyclonal antibody and anti-rabbit second antibody were products of Cell Signaling Inc (Danvers, MA, USA). Roswell Park Memorial Institute (RPMI)-1640 medium, serum free OptiMEM® medium, and 10% fetal bovine serum were obtained from Life Technologies (Carlsbad, CA, USA). siRNA targeting *hERG*, carboxyfluorescein (FAM)-labeled siRNA, and negative control siRNA were synthesized from GenePharma Inc (Shanghai, People's Republic of China). The sequences of these siRNA were: *hERG* siRNA, 5′-GAUAGGCAAACCCUACAACTT-3′; FAM-labeled siRNA, 5′-UUCUCCGAACGUGUCA CGUTT-3′; and negative control siRNA, 5′-UUCUCCGAACGUGUCACGUdTdT-3′. The human ATC HTC/3 cell line was provided by the cell bank of the Institute of Biochemistry and Cell Biology, Chinese Academy of Sciences (Shanghai, People's Republic of China). All other chemical reagents were purchased from Guangzhou Chemical Reagent Factory (Guangzhou, People's Republic of China) and were analytical grade or better unless otherwise stated.

Preparation of PAMAM-PEG-cRGD

NHS-PEG-MAL (50 mg, 10 μmol) was added to a stirred solution of cRGD (5.95 mg, 10 μmol) in a 0.1 M sodium acetate–acetic acid buffer (pH = 6.0). After stirring for 5 minutes at room temperature, PAMAM generation 4.0 dendrimer (3.55 mg, 0.25 μmol) was vigorously mixed into the reaction mixture, followed by an additional 24-hour reaction. β-mercaptoethanol 5 μL was then dropped into the mixture and stirred for another 1 hour, adjusting the pH of the reacting system to 7.0. Solvents were removed under reduced pressure and the resulting product of PAMAM-PEG-cRGD was yielded. Next, the product was dissolved in distilled water and purified by extensive dialysis using a dialysis membrane (MW cutoff = 30,000 Da) (Spectra/Por; Spectrum Laboratories Inc, Rancho Dominguez, CA, USA) against deionized water. After vacuum freeze drying, PAMAM-PEG-cRGD as a white solid was obtained.

Proton nuclear magnetic resonance (^{1}H NMR)

^{1}H NMR was analyzed by an Avance 400 MHz NMR Spectrometer (Bruker BioSpin International AG., Aegeristrasse, Zug, Swizerland). The chemical shift was interpreted as parts per million (ppm) by using a reference of D_2O (4.8 ppm) solvent peak. The structure of PAMAM-PEG-cRGD, degree of PEGylation, and conjugation of cRGD were confirmed by ^{1}H NMR.

Preparation of nano-siRNA complexes and gel retardation assay

Nano-siRNA complexes (PAMAM-siRNA and PAMAM-PEG-cRGD-siRNA) were prepared by mixing siRNA and cationic dendrimers in water at various N/P (amine/phosphate) ratios from 0–3 for 30 minutes at room temperature. Samples were then dissolved in phosphate-buffered saline (PBS) and subjected to 4% agarose gel electrophoresis at 100 V for 60 minutes in Tris-borate-ethylenediaminetetraacetic acid (EDTA) (TBE) buffer with ethidium bromide at a concentration of 5 μg/mL. Using free naked siRNA as a negative control, bands of siRNA were checked and photographed under ultraviolet light.

RiboGreen® assay of nano-siRNA complexes

After the formation of nano-siRNA complexes by the previous step, samples were then diluted with Tris-EDTA buffer (pH 7.5), and the final siRNA concentration of 0.2 μg siRNA/40 μL buffer was set by adjusting the amount of dendrimer according to the desired N/P ratio (0–3). Next, a 2 mL solution of nano-siRNA complex in each sample was transferred to a cuvette followed by the addition of 1 mL of RiboGreen (Life Technologies) reaction dye. After 5 minutes of incubation under dark conditions, the intensity of fluorescence was recorded using Picofluor fluorometer (Molecular Probes Inc, Eugene, OR, USA) at excitation/emission wavelengths of 500 nm and 525 nm, respectively. The fluorescence intensity of free naked siRNA was set as 100%, and relative fluorescence intensity was calculated. All experiments were performed in triplicate.

Dynamic light scattering and zeta potential analysis

PAMAM-PEG-cRGD was in complex with siRNA in distilled water at an N/P ratio ranging from 0.5–3. Particle size and zeta potential of the nano-siRNA complexes were determined based on dynamic light scattering techniques using a Malvern Zetasizer Nano ZS-90 (Malvern Instruments Ltd., Malvern, Worcestershire, UK) at room temperature. All parameters were measured in three runs and mean values were recorded.

Cell culture

The human ATC HTC/3 cells were cultured in RPMI-1640 medium supplemented with 10% fetal bovine serum, L-glutamine (2 mM), and penicillin-streptomycin solution. All cell lines were incubated in a humidified atmosphere of 5% CO_2 at 37°C and cells only in the exponential growth phase were eligible for the following experiments.

Cytotoxicity evaluation of dendrimers in HTC/3 cells

MTT assay was used for assessing dendrimer related cytotoxicity. HTC/3 cell suspension was centrifuged at 1000 rpm for 5 minutes before resuspending the cell pellets and seeding in a 96-well plate in which cell concentration was regulated to 1×10^5/well, and HTC/3 cells were cultivated in 5% CO_2 at 37°C overnight. The next day, each cell medium was replaced by sample medium containing PAMAM, PAMAM-PEG-cRGD, PEG, or cRGD at varying dose levels (0, 0.1, 0.5, 1, 5, and 10 μM). Each plate received an overnight incubation, after which 50 μL of MTT solution in PBS buffer was added to each well for another 4-hour treatment. With the supernatant discarded, 200 μL of dimethyl sulfoxide was applied to dissolve the formazan precipitate. Optical density was recorded at 490 nm in a microplate reader (Bio-Rad, Hercules, CA, USA). In control wells, cells received the same volume of drug-free fresh media and cell viabilities were set as 100%. All parameters were calculated three times independently and decrease of viability represented increase of cytotoxicity.

Cell transfection and siRNA delivery

PAMAM-siRNA and PAMAM-PEG-cRGD-siRNA were assembled at N/P ratios ranging from 1–5 in PBS buffer and HTC/3 cells were harvested, set at a density of 1×10^5 cells per well prior to in vitro transfection. Then 30 μL of PBS buffer containing PAMAM-siRNA, PAMAM-PEG-cRGD-siRNA, or free siRNA was mixed with 120 μL of serum-free OptiMEM medium and the final siRNA concentration of each sample was set to 100 nM. After incubation for 8 hours, the transfecting medium was replaced by fresh completed RPMI-1640 medium and incubated under normal conditions until cells were examined by confocal microscopy and flow cytometry. Free naked siRNA was used as a negative control.

Measurements of cellular uptake by confocal microscopy and flow cytometry

For measurement of the cellular uptake process, HTC/3 cells were washed with PBS buffer and fixed with 4% paraformaldehyde followed by a 15-minute treatment of DAPI after siRNA transfections. Cells were visualized using an Olympus FluoView 500 confocal microscope (Olympus Corporation, Tokyo, Japan) and FAM fluorescence was monitored, reflecting siRNA internalization and distribution in HTC/3 cells.

Transfection efficiency of siRNA in HTC/3 cells was determined by flow cytometry, before which HTC/3 cells were trypsinized, harvested by centrifugation, and resuspended under ice cold management in PBS buffer. For each run, 1×10^5 cells were analyzed on a FACSCalibur flow cytometer (BD Biosciences, Franklin Lakes, NJ, USA) for fluorescence of FAM labeled on siRNA. The proportion of FAM positive cells in each run was equivalent to the transfection efficiency of siRNA.

Gene knockdown assessments

Reverse transcription polymerase chain reaction (RT-PCR) was used to verify *hERG* silencing effects. HTC/3 cells were exposed to naked siRNA, PAMAM-siRNA, or PAMAM-PEG-cRGD-siRNA (final siRNA concentration of 100 nM) for transfection. At 24, 48, and 72 hours after transfection, total cellular RNA was isolated and synthesis of the *hERG* sequence was subsequently processed employing an ABI PCR System 9700 (Applied Biosystems Inc, Carlsbad, CA,USA). The following primers for *hERG* were used: sense strand, 5′-TCCAGCGGCTGTACTCGGGC-3′; antisense strand, 5′-TGGACCAGAAGTGGTCGGAG-3′. β-actin was used as the internal standard and primer sequences were: sense strand, 5′-AACTCCATCATG AAGTGTGA-3′; antisense strand, 5′-ACTCCTGCTTGCTGATCCAC-3′. PCR amplification setting was as follows: 95°C for 10 minutes; 94°C for 30 seconds; 56°C for 45 seconds; 72°C for 45 seconds; 40 cycles. PCR products were loaded onto 4% agarose gel electrophoresis at 80 V for approximately 40 minutes. Gels were then treated with ethidium bromide, with bands digitally photographed and quantitatively analyzed.

Antiproliferative and apoptosis assays for *hERG* knockdown

Having been treated by nano-siRNA complexes, HTC/3 cells were reseeded into a 96-well plate at a parallel density of 1×10^5/well, and each cell medium was substituted by RPMI-1640 medium containing fetal bovine serum. Another MTT assay was carried out in order to determine the antiproliferative activities of *hERG* silencing. Next, 50 μL of MTT solution was added to each well at 24, 48, and 72 hours after transfection; cells were then incubated for a further 4 hours. Dimethyl sulfoxide was added and optical density was measured. Cells untreated with siRNA were used as a blank control and considered to be 100% viable.

At 72 hours after transfection, the cell suspension was mixed thoroughly with 10 μL of fluorescein isothiocyanate-labeled annexin V and 5 μL of propidium iodide (PI) (Becton-Dickinson Inc, Franklin Lakes, NJ, USA) for 15 minutes at room temperature in the dark. Samples were analyzed by FACSCalibur flow cytometer (BD Biosciences). In general, early apoptosis cells were identified by annexin V staining but not PI (annexin V+/PI–) localizing in the right lower quadrant, whereas live cells should be stained neither by annexin V nor PI.

Morphologies of HTC/3 cells treated with nano-siRNA complexes were also viewed under an Olympus IX51 inverted light microscope (Olympus Corporation). All experiments were performed in triplicate.

Membrane interaction assay for nanocomplexes

We sought to investigate whether specific cellular ligand–receptor appetency existed in HTC/3 cells through the introduction of cRGD to a nanocarrier. Herein we used free cRGD as the competitive inhibitor in the cellular uptake process. cRGD at concentrations ranging from 0–10 μM were added to incubation media prior to siRNA transfection, after which transfection efficiencies were tested correspondingly.

Likewise, an electrostatic interaction was also needed for further exploration and a free polycationic compound, PLL at a concentration of 60 μg/mL, was employed for extrapolating the intervention of nanocarrier-related electrostatic effects.

Western blot analysis

At 6 hours after the transfection procedure, HTC/3 cells were transferred into a 96-well plate at the scheduled density of 1×10^5/ well, and cells were administered with fresh medium containing 10% fetal bovine serum for further incubation. At 24, 48, and 72 hours after transfection, total proteins were isolated by a lysis buffer (50 mM Tris-HCl, pH 7.4, 1% sodium dodecyl sulfate, 1 mM EDTA, 1 mM phenylmethanesulfonyl fluoride, 1% Triton X-100, 50 μg/mL leupeptin, 0.28 μg/mL aprotinin, and 7 μg/mL pepstatin) and quantified according to the protocol of a bicinchoninic acid protein kit (Beyotime Inc, Jiangsu, People's Republic of China). Proteins were separated by sodium dodecyl sulfate-polyacrylamide gel electrophoresis

at 100 V for approximately 50 minutes, stained with Coomassie blue (Beyotime Inc) and transferred onto nitrocellulose membranes (Whatman Inc, London, UK) afterwards. The immune combination was initiated by incubation of proteins with primary antibodies at 4°C overnight. The primary antibodies analyzed by Western blotting were: goat anti-*hERG* polyclonal antibody, goat anti-VEGF polyclonal antibody, and rabbit anti-cleaved caspase-3 polyclonal antibody. The blots were washed thoroughly and conjugated with anti-goat second antibody or anti-rabbit second antibody correspondingly. Protein bands were ultimately read by an Odyssey Scanning System (LI-COR Inc, Lincoln, NE, USA).

Statistics

The data obtained are shown as mean ± standard deviation. Statistical comparisons were made by one-way analysis of variance or Student's *t*-test using the SPSS 18.0 software (IBM Corporation, Armonk, NY, USA). A *P*-value less than 0.05 was considered to be statistically significance.

Results

Determination and characterization of PAMAM-PEG-cRGD

NHS-PEG-MAL, an important compound of the PEG provider, is also widely used as a crosslinker,[25,26] through which PEGlyation was achieved by a steady amide linkage with a reaction between primary amino groups in the PAMAM surface and NHS terminal, while cRGD was conjugated by a specific reaction between sulfhydryl and maleimide groups. It should be noted that excessive β-mercaptoethanol should be added for blockage of unreacted MAL terminal. The triblock conjugate of PAMAM-PEG-cRGD was characterized by ^{1}H NMR spectrum. Some proton peaks (Figure 1) generated from dendrimer (PAMAM), PEG, and cRGD were identified as follows: chemical shifts (δ) at 2.20–2.60 (broad, multiple peak), 3.75 (single peak), and 6.75–7.30 (broad, multiple peak) indicated the existence of PAMAM, PEG, and cRGD, respectively.

Both the degree of PEGlyation and amount of cRGD were determined by calculating the areas under these proton peaks. Generally, the amount of protons arising from dendrimer, PEG, and cRGD were 248, 434, and 4, respectively. Therefore, according to the spectrum, we finally got the result showing that one molecule of dendrimer was linked with 18.7 molecules of PEG and 11.6 molecules of cRGD.

Gel retardation and RiboGreen assay of nano-siRNA complexes

The assembly of nano-siRNA complex was confirmed by gel retardation and RiboGreen assays. Anionic siRNA oligonucleotides were neutralized, fixed, and encapsulated after being mixed with polycationic nanocarriers; thus, inhibition of electrophoretic mobility of siRNA could be seen. As shown in Figure 2A, with the increase of N/P ratios, siRNA bands gradually disappeared from agarose gels according to which optimal N/P ratios were

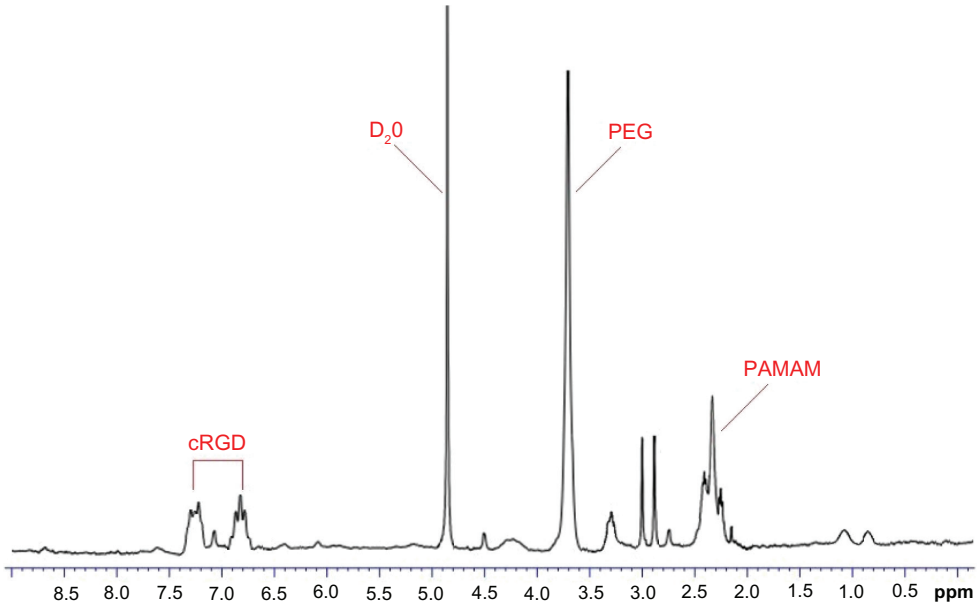

Figure 1 ^{1}H NMR spectrum of PAMAM-PEG-cRGD.
Abbreviations: ^{1}H NMR, proton nuclear magnetic resonance; cRGD, cyclic RGD; PAMAM, polyamidoamine; PEG, polyethylene glycol; ppm, parts per million.

determined. In PAMAM-siRNA, band shift was blocked at an N/P ratio higher than 3; while in PAMAM-PEG-cRGD-siRNA, hypomotility of band could be achieved at a lower N/P ratio, approximately 2. This result reveals that the surface decoration of PEG, and cRGD to some degree, slightly potentiate siRNA binding capacity for PAMAM dendrimer.

Similarly, with the gel retardation assay, the ability of the nanocarrier to complex with siRNA can be assessed by a dye exclusion method. RiboGreen, a commercial dye, was applied to detect content of free, unbound siRNA which was unfixed to the nanocarrier. The fluorescence intensity of RiboGreen decreased along with the augmenting dose of dendrimer added to siRNA oligonucleotides (Figure 2B). For PAMAM-siRNA, the formation of nano-siRNA complexes decreased RiboGreen intensities to 90%, 92%, 63%, 35%, and 24% with N/P ratios equal to 0.5, 1, 2, 2.5, and 3%, respectively; for PAMAM-PEG-cRGD-siRNA, RiboGreen intensities descended to 93%, 70%, 19%, 15%, and 18% with N/P ratios equal to 0.5, 1, 2, 2.5, and 3, respectively. When the N/P ratio reached 2, RiboGreen intensity did not fall sharply in PAMAM-PEG-cRGD-siRNA and the curve went smoothly, suggesting that the highest siRNA binding capacity was achieved in this newly established nanocarrier, with an optimal N/P ratio equal to 2. An analogous trend could be observed in PAMAM-siRNA, with an optimal N/P ratio around 3.

Dynamic light scattering and zeta potential analysis

The nanoparticle size and zeta potential of nano-siRNA complexes have some extent of significance not only in predicting interaction between nanocarrier and siRNA, but also in judging the permeability of the bypassing cell membrane. Empirically, cationic nanoparticles with diameters ranging from 100–200 nm are preferred for in vitro transfection and nanoparticles that are stable, uniform, and well-dispersed possess more effective transfection efficacies.[27,28]

Particle sizes and zeta potentials of PAMAM-PEG-cRGD-siRNA at different N/P ratios are shown in Table 1. Particle size was approximately 91.7 ± 7.1 nm at an N/P ratio of 0.5, then went up to 149.6 ± 8.7 nm at an N/P ratio of 1.5, with a modest decrease to 131.5 ± 4.5 nm at an N/P ratio of 2. However, particle sizes at N/P ratios of 2.5 and 3 were slightly larger than that at an N/P ratio of 2.

This result indicates that a proper N/P ratio is indispensible for siRNA affinity and homogenous PAMAM-PEG-cRGD-siRNA was probably formed at an N/P ratio equal to 2. An insufficient dose of dendrimer gives rise to a loose architecture; while, an overdose of dendrimer leads to a dense, concentrated structure, which increases the possibility of crosslinking for nano-siRNA complex.

Zeta potentials of PAMAM-PEG-cRGD-siRNA maintained positive values, and an ascending tendency from

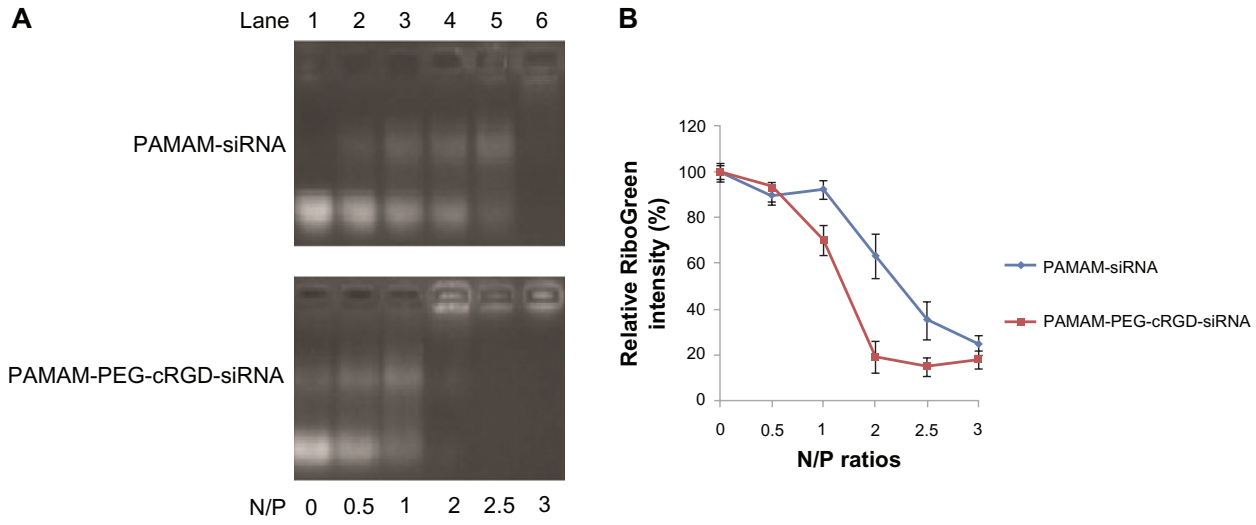

Figure 2 Features of siRNA binding capacities for nanocarriers: (**A**) Representative images of gel retardation assay for PAMAM-siRNA and PAMAM-PEG-cRGD-siRNA; (**B**) RiboGreen assay for PAMAM-siRNA and PAMAM-PEG-cRGD-siRNA.

Notes: (**A**) Lane 1, naked siRNA, N/P = 0; lane 2–6, nano-siRNA complexes at N/P ratios equal to 0.5–3.0. (**B**) Data are shown as mean ± standard deviation (n = 3) and fluorescence intensity of free naked siRNA was set as 100%.

Abbreviations: cRGD, cyclic RGD; N/P, charge ratio between amino groups and phosphate groups; PAMAM, polyamidoamine; PEG, polyethylene glycol; siRNA, short interfering RNA.

Table 1 Particle size and zeta potential of PAMAM-PEG-cRGD-siRNA at N/P ratios ranging from 0.5 to 3.0

N/P ratio	0.5	1.0	1.5	2.0	2.5	3.0
Size (nm)	91.7 ± 7.1	113.0 ± 3.6	149.0 ± 8.7	131.5 ± 4.5	148.3 ± 7.4	133.7 ± 6.0
Zeta potential (mV)	4.1 ± 1.2	5.2 ± 0.9	17.9 ± 4.1	23.9 ± 4.5	31.3 ± 5.8	38.2 ± 7.2

Abbreviations: cRGD, cyclic RGD; N/P, charge ratio between amino groups and phosphate groups; PAMAM, polyamidoamine; PEG, polyethylene glycol; siRNA, short interfering RNA.

4.1 ± 1.2 mV to 38.2 ± 7.2 mV could be easily identified at N/P ratios from 0.5 to 3. We observed an N/P ratio-dependent manner in zeta potential values in PAMAM-PEG-cRGD-siRNA. A nano-siRNA complex in a proper zeta potential is also a crux of in vitro gene transfection, in that the binding capacity of the nanocarrier is inevitably impaired at a relatively low zeta potential value, whereas excessive zeta potential aggrandizes cytotoxicity and makes inner siRNA oligonucleotides strenuous to escape from delivery system.[29]

Cytotoxicity evaluation of nanocarriers

A dendrimer exerts cytotoxicity primarily due to surface cationic groups, and is unavoidably detrimental to the stability of a negatively charged membrane, making it possible for the compromising of membrane integrity which might eventually result in cell lysis.[30] Faced with this dilemma, it is a situation of urgency to attenuate dendrimer-associated toxicity by effective surface engineerings,[31] of which PEGylation is emerging as a step of importance in chemical decoration for nanovehicles.[32,33]

An MTT assay was implemented on HTC/3 cells incubated with different concentrations of compounds. Relative cell viabilities in 24 hours were calculated (Figure 3). No significant differences were detected in these compounds under concentrations lower than 1 μM and cell viability was no lower than 75%. However, when concentrations reached 5μM, cell viability of PAMAM-NH_2 dropped to 50.9% ± 4.9%, displaying higher cytotoxicity when compared with PAMAM-PEG-cRGD, PEG, and cRGD ($P < 0.01$). PAMAM-NH_2 at a concentration of 10 μM diminished the percentage of viable cells to 40.7% ± 6.3%, which was statistically lower than the cell viability recorded in other compounds at the same concentration ($P < 0.01$), yet cells exposed to PAMAM-PEG-cRGD retained 80% cell viability above concentrations lower than 10 μM.

This result demonstrates a comparably low cytotoxicity after conjugation of PEG and cRGD, with respect to unmodified PAMAM. It should be stressed that PAMAM-PEG-cRGD, cRGD, or PEG might be markedly cytotoxic under concentrations much higher than 10 μM. But in our work we should put more emphasis on cytotoxic properties ranging from 0–1 μM given that the final siRNA concentration for in vitro transfection was fixed at 100 nM. The cytotoxicity data of PAMAM-PEG-cRGD showed that HTC/3 cells were alive under experimental doses, which would not consequently bring apparent interferences to transfection and antiproliferative assays.

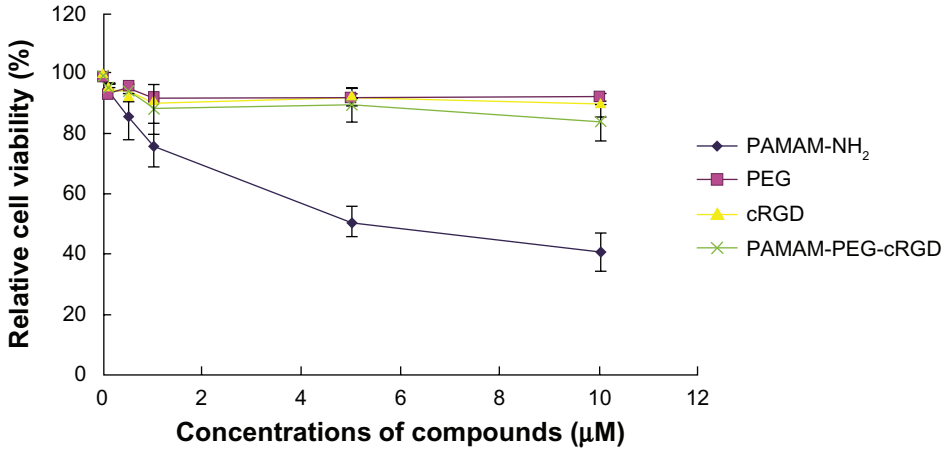

Figure 3 Relative cell viabilities for HTC/3 cells incubated with PAMAM-NH_2, PEG, cRGD, and PAMAM-PEG-cRGD at 0, 0.1, 0.5, 1, 5, and 10 μM.
Notes: Viability of cells treated with fresh media was set as 100%. Data are expressed as mean ± standard deviation (n = 3).
Abbreviations: cRGD, cyclic RGD; PAMAM, polyamidoamine; PEG, polyethylene glycol.

In vitro transfection and cellular uptake

FAM-labeled *hERG*-siRNA was delivered to HTC/3 cells via a nanocarrier transfecting system, for which transfection efficiency and cellular siRNA distribution were accomplished using flow cytometry and confocal microscopy, respectively. The results of this step are illustrated in Figure 4. For nanocarriers, the transfection efficiencies varied corresponding to N/P ratios. Not surprisingly, naked siRNA failed to enter the cells (Figure 4A). For PAMAM-siRNA, only a minority of FAM-labeled siRNAs penetrated into the cells, and the population of FAM positive cells was 10.9% ± 6.4% when the N/P ratio was 3 (Figure 4B). For PAMAM-PEG-cRGD-siRNA, we observed homogenous distribution of siRNA mainly in cytoplasm through confocal microscopy 6 hours after transfection, with transfection efficiency up to 68% on the condition that the N/P ratio was 3.5 (Figure 4C). Our findings provide strong evidence showing that siRNA complexed with PAMAM-PEG-cRGD exhibits excellent cellular internalization.

Basically, a higher N/P ratio leads to higher transfection efficiency, based on the fact that a higher N/P ratio results in higher cationic density, which is essential for breaching the cell membrane barrier. However, for each nano-siRNA complex, we did observe an optimal transfecting N/P ratio (Figure 4D) in which transfection efficiency reached its peak: the transfection efficiencies were the highest if N/P ratios were equal to 4.5 and 3.5 in PAMAM-siRNA and PAMAM-PEG-cRGD-siRNA, respectively. In terms of

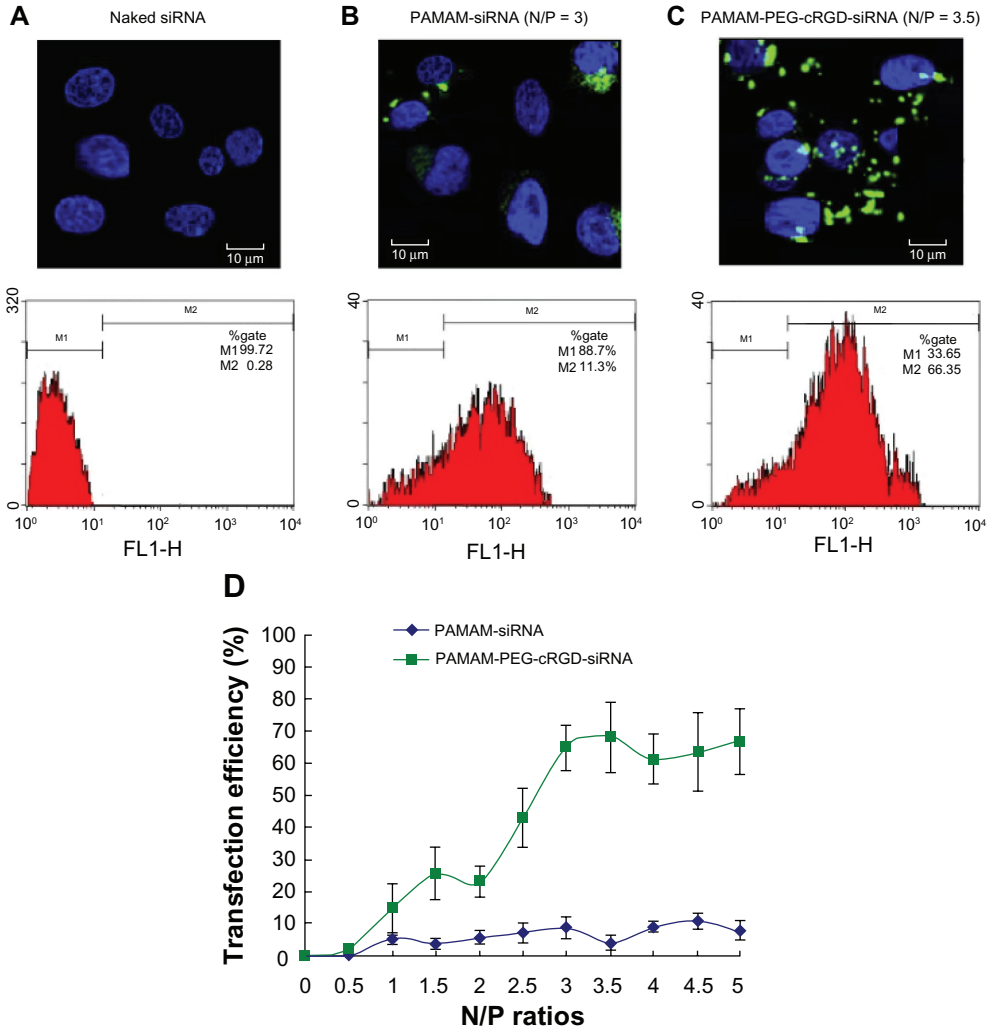

Figure 4 Results of siRNA transfection and cellular uptake: (**A**) Representative confocal images and flow cytometry histograms of HTC/3 cells transfected with naked siRNA; (**B**) PAMAM-siRNA complexes at an N/P ratio equal to 3; (**C**) PAMAM-PEG-cRGD-siRNA complexes at an N/P ratio equal to 3.5; (**D**) Transfection efficiencies of dendritic nano-siRNA complexes at various N/P ratios.

Notes: The nucleus was stained by DAPI in blue fluorescence and siRNA was labeled with FAM in green fluorescence (scale bar in 10 μm). Data are presented as mean ± standard deviation (n = 3).

Abbreviations: cRGD, cyclic RGD; DAPI, 4,6-diamidino-2-phenylindole; FAM, carboxyfluorescein; N/P, charge ratio between amino groups and phosphate groups; PAMAM, polyamidoamine; PEG, polyethylene glycol; siRNA, short interfering RNA.

siRNA uptake and distribution, a range of critical aspects should be addressed, including particle size, homogeneity, zeta potential, siRNA concentration, incubation conditions, different cell lines, and so forth.[27–29] One reasonable explanation for the optimal transfecting N/P ratio is that cellular endocytosis favors foreign particles that are well-dispersed and homogenous.

RT-PCR gene knockdown assessment

We selected PAMAM-siRNA at an N/P ratio of 4.5 and PAMAM-PEG-cRGD-siRNA at an N/P ratio of 3.5 to estimate silencing activity through RT-PCR where *hERG* messenger RNA (mRNA), a product of 575 bp was yielded, with β-actin (247 bp) as the internal standard. As shown in Figure 5A, we confirmed again that human ATC HTC/3 cells expressed *hERG*, and naked siRNA had little influence on *hERG* mRNA silencing. PAMAM-siRNA restrained *hERG* expression to 66.7%–77.7% of untreated values 24 to 72 hours after transfection. On the other hand, siRNA carried by triblock suppressed the molecular level of *hERG* targeted genes to 26.3%–47.3% of control values. It was remarkable that siRNA in assembly with PAMAM-PEG-cRGD exhibited more powerful gene silencing effects when compared with the parent PAMAM-NH_2 (Figure 5B). In addition, we noticed that the knockdown effects in both nanocarriers lasted over 3 days, implying that complexation of siRNA to dendrimer was a beneficial approach to prolong siRNA stability and duration in cytoplasm without abrogating silencing efficacy.

Antiproliferative and apoptosis effects of *hERG* knockdown

The treatment of PAMAM-PEG-cRGD-siRNA (N/P ratio = 3.5, final concentration of siRNA = 100 nm) for human ATC HTC/3 cells presented an antineoplastic therapeutic effect on the basis of growth suppression, according to data collected from MTT assays (Figure 6A). It should be highlighted again that experimental concentrations in this procedure were within the nontoxic window of PAMAM-PEG-cRGD for HTC/3 cells; that is to say, we might ascribe antiproliferative effects primarily to siRNA targeting *hERG*. The knockdown of *hERG* reversed proliferation in a time-dependent manner, as the rate of viable cells gradually downgraded to 58.3% ± 6.4% 72 hours after the administration of nano-siRNA complexes (Figure 6A and B). RNA interference of *hERG* also modulated HTC/3 cell apoptosis, since a 72-hour treatment of nano-siRNA significantly increased the portion of early apoptosis cells (annexin V+/PI–) versus the control (15.5% ± 0.8% versus 3.2% ± 0.3%, $P < 0.01$, Figure 6C).

Membrane interaction of nano-siRNA complexes

The initial access of cellular uptake of nano-siRNA complexes includes membrane interaction, in which electrostatic force as well as specific ligand–receptor mechanisms might be involved. We loaded the nanocarrier with a cRGD sequence conjugated for the sake of intelligent recognition of integrin protein in HTC/3 cells. To discern this hypothesis, free excessive cRGD and PLL were added

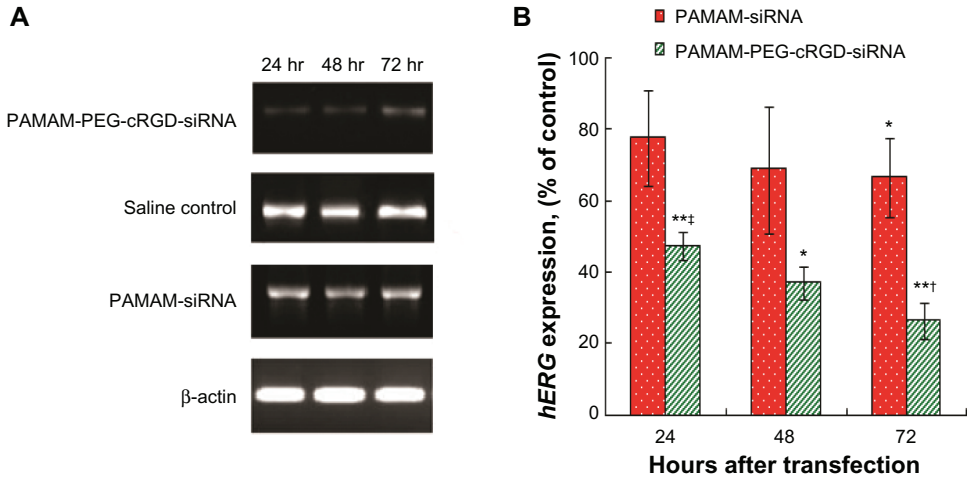

Figure 5 (**A**) Representative RT-PCR agarose gel electrophoresis images and (**B**) relative expression percentages of *hERG* at 24, 48, and 72 hours after administration of PAMAM-PEG-cRGD-siRNA or PAMAM-siRNA.

Notes: The expression of *hERG* at baseline level (fresh medium, 0 hours) was set to be 100%. Data are presented as mean ± standard deviation (n = 3). *$P < 0.05$ when compared with control; **$P < 0.01$ when compared with control; †$P < 0.05$ when compared with PAMAM-siRNA; ‡$P < 0.01$ when compared with PAMAM-siRNA.

Abbreviations: cRGD, cyclic RGD; *hERG*, human ether-à-go-go-related gene; hr, hours; PAMAM, polyamidoamine; PEG, polyethylene glycol; RT-PCR, reverse transcription polymerase chain reaction; siRNA, short interfering RNA.

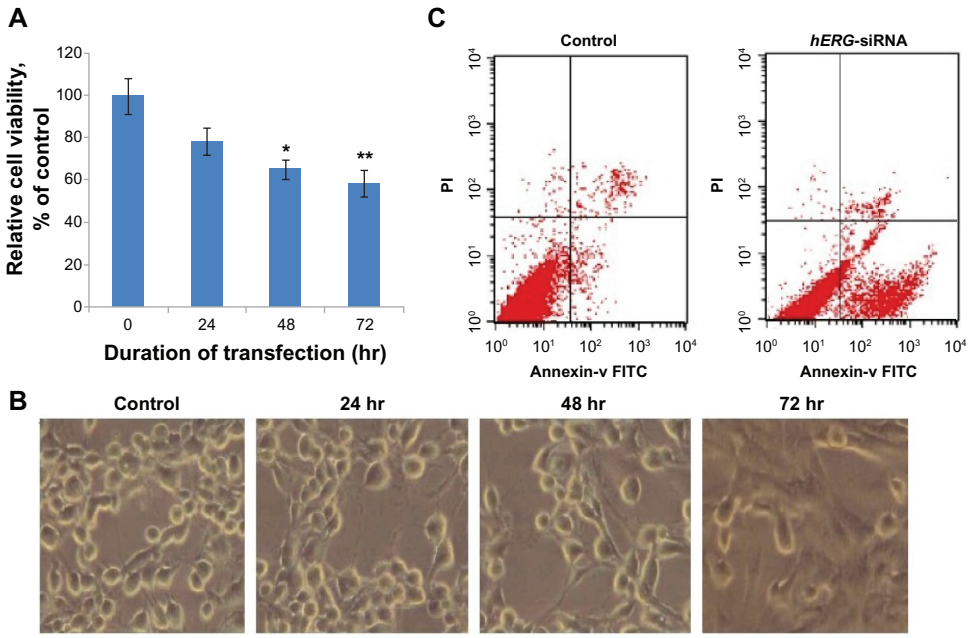

Figure 6 Antiproliferative and apoptosis effects of *hERG* knockdown: (**A**) Relative viabilities for HTC/3 cells treated with PAMAM-PEG-cRGD-siRNA within 72 hours; (**B**) Microscope images of HTC/3 cells transfected by nano-siRNA over 72 hours; (**C**) Representative images of flow cytometry of annexin V/PI staining for HTC/3 cells after 72 hours of *hERG*-siRNA transfection.

Notes: Viability of cells treated with fresh media was set as 100%. *$P < 0.05$ when compared with the control at the same duration; **$P < 0.01$ when compared with the control at the same duration. Data are presented as mean ± standard deviation (n = 3).

Abbreviations: cRGD, cyclic RGD; FITC, fluorescein isothiocyanate; *hERG*, human ether-a-go-go-related gene; hr, hours; PAMAM, polyamidoamine; PEG, polyethylene glycol; PI, propidium iodide; siRNA, short interfering RNA.

as competitive inhibitors for further co-incubation. Firstly, we had to test cytotoxicity data in HTC/3 cells treated with free cRGD and PLL under experimental concentrations, which were 0–10 μM and 60 μg/mL, respectively; the data provided evidence that no severe interference occurred. The transfection efficiency of cells treated with PAMAM-PEG-cRGD-siRNA at an N/P ratio of 3.5 in the absence of inhibitors was used as the control; this cellular uptake was set as 100% as a reference. As shown in Figure 7, the proportion of FAM-positive cells dropped to approximately 83% of the control value when HTC/3 cells were co-treated with 10 μM of free cRGD, and this resulting difference was statistically significant ($P < 0.05$). Additionally, the relative cellular uptake percentage of cells treated with PLL (60 μg/mL) also significantly declined to 55% of the control level ($P < 0.05$). We also observed that free cRGD lowered cellular

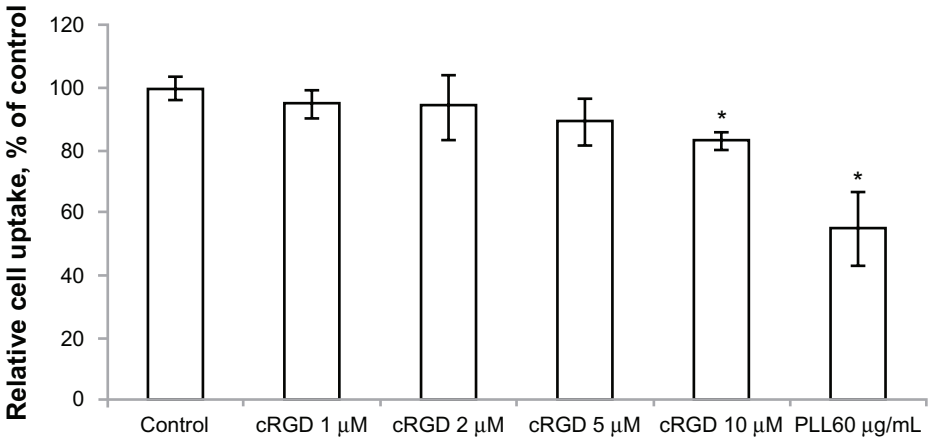

Figure 7 Relative cellular uptake of nano-siRNA complexes for HTC/3 cells treated with free excessive cRGD and PLL.

Notes: Transfection efficiency of cells treated with nano-siRNA without inhibitors was set as 100% cellular uptake. *$P < 0.05$ when compared with the control. Data are presented as mean ± standard deviation (n = 3).

Abbreviations: cRGD, cyclic RGD; PLL, poly(L-lysine); siRNA, short interfering RNA.

uptake of nano-siRNA complexes in a dose-dependent manner. Therefore, this result indicated that the introduction of cRGD boosted cellular uptake of nano-siRNA complexes by cRGD-integrin binding, and the electrostatic effect was also an essential factor for endocytosis in HTC/3 cells.

Western blot analysis

Having noticed that *hERG* had a profound, complicated signaling network targeting carcinogenesis, several pathological proteins were studied by with Western blotting. Both VEGF and caspase-3 are known to be far-reaching and impactful in cell survival control, and the question of whether *hERG* has functional interactions with these factors is raised. Silencing of *hERG* was confirmed again by Western blot with sharp downregulation of *hERG* in protein level (Figure 8A). As a gene encoding specific K^+ channel,[10] *hERG* deprivation gave rise to complete downregulation of VEGF protein in HTC/3 cells as compared to the control (Figure 8B), suggesting that the action of VEGF secretion required the presence of *hERG*, at least partially. Silencing *hERG* brought about programed cell death in HTC/3 cells, and activation of caspase-3, pivotal in triggering a cascade of the apoptosis pathway,[34] was involved (Figure 8C). However, these results are still tentative and imperfect, and the question how *hERG* mRNA or *hERG* protein physiologically interacts with VEGF or caspase-3 is unanswered. The details of the signaling network of *hERG*, caspase, and angiogenesis at the molecular level remain sparse to date, and more intensive investigations are needed.

Discussion

Dendrimers open an exciting avenue of research and exploration for siRNA delivery, however, there are still critical challenges such as existing cytotoxicity, relatively poor cellular uptake, stiff endosomal escape.[35] In this study, we constructed a novel triblock nanocarrier PAMAM-PEG-cRGD, in which PAMAM acted as the dendrimer core providing cationic strength sufficient for penetrating the cell membrane, PEG as the improver of biocompatibility, and cRGD as the enhancer of endocytosis and cancer targeting. Undoubtedly, the interaction of siRNA and dendrimer is complicated and refers to numerous factors including generation, cationic strength, particle size, pH, architecture.

According to the data obtained from the gel retardation assay, and particle size and zeta potential analysis, N/P ratios of approximately 2 and 3 were optimal for the binding capacities of siRNA in PAMAM-PEG-cRGD and PAMAM, respectively. Hence, we validated that adequate size and ionic density (N/P ratio) were needed for potent siRNA binding. There are reports showing that PEGlyation might sometimes

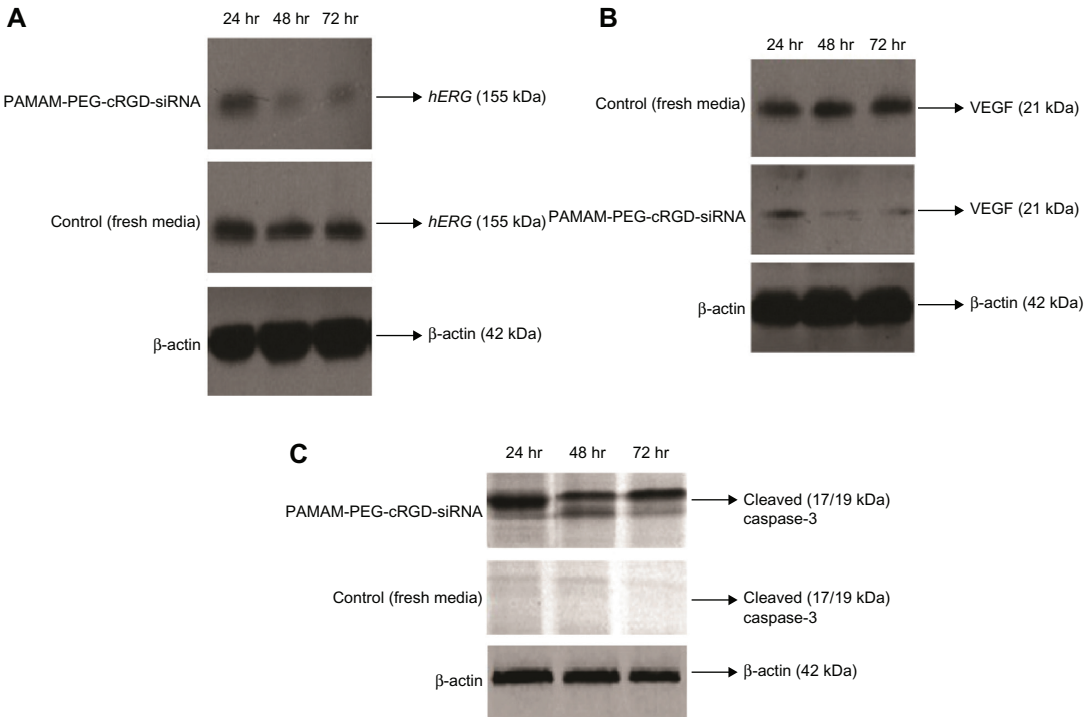

Figure 8 Representative Western blot agarose images of (**A**) *hERG* protein, (**B**) VEGF, and (**C**) caspase-3 within 72 hours by *hERG* silencing in HTC/3 cells.
Abbreviations: cRGD, cyclic RGD; *hERG*, human ether-a-go-go-related gene; hr, hours; PAMAM, polyamidoamine; PEG, polyethylene glycol; siRNA, short interfering RNA; VEGF, vascular endothelial growth factor.

shelter cationic surfaces and thus plague the bioactivity of nucleic acids,[36–38] but conversely, the PEG modification slightly enhanced dendrimer–siRNA linking in our work, indicating that not only cationic density, but also polymeric architecture played a vital role in siRNA binding. However, an excellent binding does not guarantee a satisfactory cellular internalization profile. The optimal N/P ratio detected by physiochemical parameters might be different from the best N/P ratio determined by cellular uptake, because there was membrane barrier with which nanoparticles also interacted intricately. An effective nano-siRNA complex was formed in PAMAM generation 4.0, but the transfection efficiency was weak, and this finding was consistent with Patil et al's work, in which commercial generation 4.0 PAMAM-NH_2 failed to deliver siRNA into cells, partially owing to nanofibers caused by crosslinking.[39]

To elicit RNAi, siRNA has to be released from carriers to perform the task in cytoplasm. High cellular uptake does not ensure powerful silencing effects.[40,41] A representative example is PLL, which possesses high affinity to siRNA, but lack of gene knockdown actions, mainly as a result of the deficiency of tertiary amine groups required for a proton sponge effect.[42,43] Reports provided by molecular dynamics stimulations also gave critical evidence for proton sponge theory in PAMAM, elucidating that successful transfection requires a proper cationic environment where the ratio of dendrimer to siRNA should neither be too high nor too low.[44–46]

Integrin, a known cell surface receptor and potential therapeutic target, is overexpressed in ATC.[47] In our present work, cRGD–integrin intimacy was seen, mediating the promotion of endocytosis and our data agreed with the report from Waite and Roth, in which the insertion of cRGD to PAMAM generation 5.0 enhanced siRNA uptake and inhibited adhesion in a concentration-dependent manner.[48] It should be noted that some investigators reported RGD peptides alone might suppress tumor growth and induce programmed cell death,[49,50] but under our experimental conditions in which the concentration of cRGD was relatively low, no obvious impact on cell viability was observed in HTC/3 cells in regards to cRGD attachment.

The in vitro to in vivo correlation of biocompatibility and transfection profile remains challenging. All procedures in this study are in vitro experiments at this stage. Multiple in vivo cytotoxic mechanisms are rooted in different cell lines, tissue origins, administrative methods, and so on. For example, neurons or cardiomyocytes might be less resistant to dendrimer toxicity in comparison to proliferative cancerous cells.[51] The administrative pathway also dramatically influences the effectiveness of siRNA therapy in vivo, and different administrative approaches result in different dose ranges. Intravenous administration might manifest more severe off-target complications than oral or local application. It was observed that when intravenously administered, generation 4.0 PAMAM-NH_2 was not tolerated at doses higher than 10 mg/kg in rats.[52] But it seems that the biocompatiblity of cationic dendrimers increases approximately ten-fold when administered locally or through the gastrointestinal tract, making it possible to deliver higher doses of siRNA by dendrimer.[53] Moreover, we have to take into account the dynamic pharmacokinetics for animal applications, as dendrimer or siRNA can be eliminated or degraded by the kidney and liver. Few established relationships exist to deduce transfection behavior from in vitro data in in vivo studies. Difficulties should be conquered by the optimization of dose range or administration approaches, more excellent surface chemistries for bioavailability, and transporting mighty siRNAs.

Therapeutic approaches for ATC are far from ideal. The understanding of molecular pathogenesis of ATC hold promises for gene therapy. *hERG*, encoding specific dependent K^+ channels, participates in the depolarization of membrane potentials and retards the cell cycle by partial blockage in the G1 phase in many cancerous cells.[54,55] *hERG* dependent K^+ channels are shut off at membrane potentials below a threshold of –60 mV while classical inwardly rectifying channels switch on at more negative potentials which are particularly depolarized during the G1 phase.[56] Nevertheless, *hERG* K^+ channel-dependent hyperpolarization appears to be fundamental for S phase progression. Hyperpolarization stimulates Ca^{2+} influx, permits synthesis of mitogenic factors and provides the electrical gradient essential for Na^+-dependent transport of metabolic substrates and ions necessary for DNA synthesis.[57] Abundant expression of *hERG* channels is therefore expected to cause loss of proliferative control.[57] On the other hand, the promoter region of the *hERG* gene harbors multiple binding sites for oncoproteins, such as specificity protein 1, nuclear factor kappa light chain enhancer, and tumor suppressor protein Nkx3.1.[58] Overexpression of *hERG* alters the resting membrane potentials of cancerous cells toward more depolarized values and repolarizes them at the end of the G1 phase, thereby facilitating cell cycle progression and thus arousing proliferation.[59]

By the silencing method, we found that downregulation of *hERG* caused cell death and apoptosis in HTC/3 cells. Moreover, *hERG* silencing resulted in the reduction of VEGF secretion and activation of caspase-3. In HL-1 cardiomyocytes, *hERG* blockage evokes apoptosis via the

endoplasmic reticulum pathway, involving phosphorylation of p38 mitogen-activated protein kinase, which activates the growth arrest and DNA damage-induced gene 153/c/EBP homologous protein, accelerating the activation of caspase-3.[60] Cherubini et al[61] reported that in SH-SY5Y glioma cells, *hERG*, integrin β_1, and focal adhesion kinase formed a complex, and the activation of *hERG* directly attributed to the phosphorylation of focal adhesion kinase, which stirs up survival signaling and prevents apoptosis. Pillozzi et al[62] also clarified that *hERG* K^+ channel, VEGF receptor-1(FLT-1), and integrin β_1 formed a signaling complex, modulating cell proliferation, adhesion, and invasion in human acute myelocytic leukemia cells. However, a more detailed signaling transduction pathway and a systematic understanding of *hERG* in ATC remain unclear and we are dedicated to future studies.

Conclusion

In this study, we initially proposed a nanoscale dendrimer–siRNA delivery system to elicit the gene silencing effect of *hERG* in human ATC cells in vitro. This novel triblock polymer, PAMAM-PEG-cRGD, exhibits little cytotoxicity, effective transfection efficiency, "smart" cancer targeting, and therefore is a successful siRNA nanocarrier. Moreover, knockdown of *hERG* inhibits cell growth and induces apoptosis in ATC cells in vitro.

Acknowledgments

The present work was supported by the National High Technology Research and Development Program of China (Grant Number 2007AA021904) and the Science and Technology Planning Project of Guangdong Province (Grant Number 2010B031600055).

Disclosure

The authors report no conflicts of interest in this work.

References

1. Aagaard L, Rossi JJ. RNAi therapeutics: principles, prospects and challenges. *Adv Drug Deliv Rev*. 2007;59(2–3):75–86.
2. Burnett JC, Rossi JJ, Tiemann K. Current progress of siRNA/shRNA therapeutics in clinical trials. *Biotechnol J*. 2011;6(9):1130–1146.
3. Whitehead KA, Langer R, Anderson DG. Knocking down barriers: advances in siRNA delivery. *Nat Rev Drug Discov*. 2009;8(2):129–138.
4. Kukowska-Latallo JF, Bielinska AU, Johnson J, Spindler R, Tomalia DA, Baker JR Jr. Efficient transfer of genetic material into mammalian cells using Starburst polyamidoamine dendrimers. *Proc Natl Acad Sci U S A*. 1996;93(10):4897–4902.
5. Liu XX, Rocchi P, Qu FQ, et al. PAMAM dendrimers mediate siRNA delivery to target Hsp27 and produce potent antiproliferative effects on prostate cancer cells. *Chem Med Chem*. 2009;4(8):1302–1310.
6. Kim ID, Shin JH, Kim SW, et al. Intranasal delivery of HMGB1 siRNA confers target gene knockdown and robust neuroprotection in the postischemic brain. *Mol Ther*. 2012;20(4):829–839.
7. Zhou J, Neff CP, Liu X, et al. Systemic administration of combinatorial dsiRNAs via nanoparticles efficiently suppresses HIV-1 infection in humanized mice. *Mol Ther*. 2011;19(12):2228–2238.
8. Arima H, Tsutsumi T, Yoshimatsu A, et al. Inhibitory effect of siRNA complexes with polyamidoamine dendrimer/α-cyclodextrin conjugate (generation 3, G3) on endogenous gene expression. *Eur J Pharm Sci*. 2011;44(3):375–384.
9. Neff RL, Farrar WB, Kloos RT, Burman KD. Anaplastic thyroid cancer. *Endocrinol Metab Clin North Am*. 2008;37(2):525–538.
10. Sanguinetti MC, Tristani-Firouzi M. *hERG* potassium channels and cardiac arrhythmia. *Nature*. 2006;440(7083):463–469.
11. Wadhwa S, Wadhwa P, Dinda AK, Gupta NP. Differential expression of potassium ion channels in human renal cell carcinoma. *Int Urol Nephrol*. 2009;41(2):251–257.
12. Masi A, Becchetti A, Restano-Cassulini R, et al. *hERG1* channels are overexpressed in glioblastoma multiforme and modulate VEGF secretion in glioblastoma cell lines. *Br J Cancer*. 2005;93(7):781–792.
13. Pillozzi S, Brizzi MF, Balzi M, et al. *hERG* potassium channels are constitutively expressed in primary human acute myeloid leukemias and regulate cell proliferation of normal and leukemic hemopoietic progenitors. *Leukemia*. 2002;16(9):1791–1798.
14. Wang Y, Zhang Y, Yang L, et al. Arsenic trioxide induces the apoptosis of human breast cancer MCF-7 cells through activation of caspase-3 and inhibition of *hERG* channels. *Exp Ther Med*. 2011;2(3):481–486.
15. Pardo LA, Contreras-Jurado C, Zientkowska M, Alves F, Stühmer W. Role of voltage-gated potassium channels in cancer. *J Membr Biol*. 2005;205(3):115–124.
16. Rust WL, Carper SW, Plopper GE. The promise of integrins as effective targets for anticancer agents. *J Biomed Biotechnol*. 2002;2(3):124–130.
17. Cai W, Chen X. Anti-angiogenic cancer therapy based on integrin alphaVbeta3 antagonism. *Anticancer Agents Med Chem*. 2006;6(5):407–428.
18. Aumailley M, Gurrath M, Müller G, Calvete J, Timpl R, Kessler H. Arg-Gly-Asp constrained within cyclic pentapeptides: Strong and selective inhibitors of cell adhesion to vitronectin and laminin fragment P1. *FEBS Lett*. 1991;291(1):50–54.
19. Nabors LB, Mikkelsen T, Rosenfeld SS, et al. Phase I and correlative biology study of cilengitide in patients with recurrent malignant glioma. *J Clin Oncol*. 2007;25(13):1651–1657.
20. Reardon DA, Fink KL, Mikkelsen T, et al. Randomized phase II study of cilengitide, an integrin-targeting arginine-glycine-aspartic acid peptide, in recurrent glioblastoma multiforme. *J Clin Oncol*. 2008;26(34):5610–5617.
21. Reardon DA, Neyns B, Weller M, Tonn JC, Nabors LB, Stupp R. Cilengitide: an RGD pentapeptide αvβ3 and αvβ5 integrin inhibitor in development for glioblastoma and other malignancies. *Future Oncol*. 2011;7(3):339–354.
22. Lee MH, Kim JY, Han JH, et al. Direct fluorescence monitoring of the delivery and cellular uptake of a cancer-targeted RGD peptide-appended naphthalimide theragnostic prodrug. *J Am Chem Soc*. 2012;134(30):12668–12674.
23. Danhier F, Pourcelle V, Marchand-Brynaert J, Jérôme C, Feron O, Préat V. Targeting of tumor endothelium by RGD-grafted PLGA-nanoparticles. *Methods Enzymol*. 2012;508:157–175.
24. Boswell CA, Eck PK, Regino CA, et al. Synthesis, characterization, and biological evaluation of integrin alphaVbeta3-targeted PAMAM dendrimers. *Mol Pharm*. 2008;5(4):527–539.
25. Wang YY, Lü LX, Shi JC, Wang HF, Xiao ZD, Huang NP. Introducing RGD peptides on PHBV films through PEG-containing cross-linkers to improve the biocompatibility. *Biomacromolecules*. 2011;12(3):551–559.
26. Natarajan A, Xiong CY, Albrecht H, DeNardo GL, DeNardo SJ. Characterization of site-specific ScFv PEGylation for tumor-targeting pharmaceuticals. *Bioconjug Chem*. 2005;16(1):113–121.

27. Pedraza CE, Bassett DC, McKee MD, Nelea V, Gbureck U, Barralet JE. The importance of particle size and DNA condensation salt for calcium phosphate nanoparticle transfection. *Biomaterials*. 2008;29(23):3384–3392.
28. Patil Y, Panyam J. Polymeric nanoparticles for siRNA delivery and gene silencing. *Int J Pharm*. 2009;367(1–2):195–203.
29. Wagner E, Cotten M, Foisner R, Birnstiel ML. Transferrin-polycation-DNA complexes: the effect of polycations on the structure of the complex and DNA delivery to cells. *Proc Natl Acad Sci U S A*. 1991;88(10):4255–4259.
30. Agashe HB, Dutta TD, Garg M, Jain NK. Investigations on the toxicological profile of functionalized fifth-generation poly(propyleneimine) dendrimer. *J Pharm Pharmacol*. 2006;58(11):1491–1498.
31. Wang YX, Robertson JL, Spillman WB Jr, Claus RO. Effects of the chemical structure and the surface properties of polymeric biomaterials on their biocompatibility. *Pharm Res*. 2004;21(8):1362–1373.
32. Wang W, Xiong W, Wan J, Sun X, Xu H, Yang X. The decrease of PAMAM dendrimer-induced cytotoxicity by PEGylation via attenuation of oxidative stress. *Nanotechnology*. 2009;20(10):105103.
33. Gajbhiye V, Vijayaraj Kumar P, Kumar Tekade R, Jain NK. Pharmaceutical and biomedical potential of PEGylated dendrimers. *Curr Pharm Des*. 2007;13(4):415–429.
34. Fiandalo MV, Kyprianou N. Caspase control: protagonists of cancer cell apoptosis. *Exp Oncol*. 2012;34(3):165–175.
35. Raviña M, Paolicelli P, Seijo B, Sanchez A. Knocking down gene expression with dendritic vectors. *Mini Rev Med Chem*. 2010;10(1): 73–86.
36. Deshpande MC, Davies MC, Garnett MC, et al. The effect of poly(ethylene glycol) molecular architecture on cellular interaction and uptake of DNA complexes. *J Control Release*. 2004;97(1):143–156.
37. Li SD, Chono S, Huang L. Efficient gene silencing in metastatic tumor by siRNA formulated in surface-modified nanoparticles. *J Control Release*. 2008;126(1):77–84.
38. Li W, Huang Z, MacKay JA, Grube S, Szoka FC Jr. Low-pH-sensitive poly(ethylene glycol) (PEG)-stabilized plasmid nanolipoparticles: effects of PEG chain length, lipid composition and assembly conditions on gene delivery. *J Gene Med*. 2005;7(1):67–79.
39. Patil ML, Zhang M, Minko T. Multifunctional triblock nanocarrier (PAMAM-PEG-PLL) for the efficient intracellular siRNA delivery and gene silencing. *ACS Nano*. 2011;5(3):1877–1887.
40. Chandna P, Saad M, Wang Y, et al. Targeted proapoptotic anticancer drug delivery system. *Mol Pharm*. 2007;4(5):668–678.
41. Patil ML, Zhang M, Taratula O, Garbuzenko OB, He H, Minko T. Internally cationic polyamidoamine PAMAM-OH dendrimers for siRNA delivery: effect of the degree of quaternization and cancer targeting. *Biomacromolecules*. 2009;10(2):258–266.
42. Inoue Y, Kurihara R, Tsuchida A, et al. Efficient delivery of siRNA using dendritic poly(L-lysine) for loss-of-function analysis. *J Control Release*. 2008;126(1):59–66.
43. Kano A, Moriyama K, Yamano T, Nakamura I, Shimada N, Maruyama A. Grafting of poly(ethylene glycol) to poly-lysine augments its lifetime in blood circulation and accumulation in tumors without loss of the ability to associate with siRNA. *J Control Release*. 2011;149(1):2–7.
44. Karatasos K, Posocco P, Laurini E, Pricl S. Poly(amidoamine)-based dendrimer/siRNA complexation studied by computer simulations: effects of pH and generation on dendrimer structure and siRNA binding. *Macromol Biosci*. 2012;12(2):225–240.
45. Ouyang D, Zhang H, Parekh HS, Smith SC. The effect of pH on PAMAM dendrimer-siRNA complexation: endosomal considerations as determined by molecular dynamics simulation. *Biophys Chem*. 2011;158(2–3):126–133.
46. Jensen LB, Pavan GM, Kasimova MR, et al. Elucidating the molecular mechanism of PAMAM-siRNA dendriplex self-assembly: effect of dendrimer charge density. *Int J Pharm*. 2011;416(2):410–418.
47. Dahlman T, Grimelius L, Wallin G, Rubin K, Westermark K. Integrins in thyroid tissue: upregulation of alpha2beta1 in anaplastic thyroid carcinoma. *Eur J Endocrinol*. 1998;138(1):104–112.
48. Waite CL, Roth CM. PAMAM-RGD conjugates enhance siRNA delivery through a multicellular spheroid model of malignant glioma. *Bioconjug Chem*. 2009;20(10):1908–1916.
49. Huang TC, Huang HC, Chang CC, et al. An apoptosis-related gene network induced by novel compound-cRGD in human breast cancer cells. *FEBS Lett*. 2007;581(18):3517–3522.
50. Yang W, Meng L, Wang H, et al. Inhibition of proliferative and invasive capacities of breast cancer cells by arginine-glycine-aspartic acid peptide in vitro. *Oncol Rep*. 2006;15(1):113–117.
51. Albertazzi L, Gherardini L, Brondi M, et al. In vivo distribution and toxicity of PAMAM dendrimers in the central nervous system depend on their surface chemistry. *Mol Pharm*. 2013;10(1):249–260.
52. Roberts JC, Bhalgat MK, Zera RT. Preliminary biological evaluation of polyamidoamine (PAMAM) Starburst dendrimers. *J Biomed Mater Res*. 1996;30(1):53–65.
53. Sadekar S, Ghandehari H. Transepithelial transport and toxicity of PAMAM dendrimers: implications for oral drug delivery. *Adv Drug Deliv Rev*. 2012;64(6):571–588.
54. Bianchi L, Wible B, Arcangeli A, et al. *hERG* encodes a K^+ current highly conserved in tumors of different histogenesis: a selective advantage for cancer cells? *Cancer Res*. 1998;58(4):815–822.
55. Shao XD, Wu KC, Guo XZ, Xie MJ, Zhang J, Fan DM. Expression and significance of *hERG* protein in gastric cancer. *Cancer Biol Ther*. 2008;7(1):45–50.
56. Ishihara K, Hiraoka M. Gating mechanism of the cloned inward rectifier potassium channel from mouse heart. *J Membr Biol*. 1994;142(1):55–64.
57. Wonderlin WF, Strobl JS. Potassium channels, proliferation and G1 progression. *J Membr Biol*. 1996;154(2):91–107.
58. Lin H, Xiao J, Luo X, et al. Overexpression *hERG* K(+) channel gene mediates cell-growth signals on activation of oncoproteins SP1 and NF-kappaB and inactivation of tumor suppressor Nkx3.1. *J Cell Physiol*. 2007;212(1):137–147.
59. Jehle J, Schweizer PA, Katus HA, Thomas D. Novel roles for *hERG* K(+) channels in cell proliferation and apoptosis. *Cell Death Dis*. 2011;2:e193.
60. Eiras S, Fernández P, Piñeiro R, Iglesias MJ, González-Juanatey JR, Lago F. Doxazosin induces activation of GADD153 and cleavage of focal adhesion kinase in cardiomyocytes route to apoptosis. *Cardiovasc Res*. 2006;71(1):118–128.
61. Cherubini A, Hofmann G, Pillozzi S, et al. Human ether-a-go go-related gene 1 channels are physically linked to beta1 integrins and modulate adhesion dependent signaling. *Mol Biol Cell*. 2005;16(6):2972–2983.
62. Pillozzi S, Brizzi MF, Bernabei PA, et al. VEGFR-1 (FLT-1), beta1 integrin, and *hERG* K^+ channel for a macromolecular signaling complex in acute myeloid leukemia: role in cell migration and clinical outcome. *Blood*. 2007;110(4):1238–1250.